Nationaal Lucht- en Ruimtevaartlaboratorium
National Aerospace Laboratory NLR

NLR TP 96312

Propeller-wing interference effects at low speed conditions

L.G.M. Custers

DOCUMENT CONTROL SHEET

	ORIGINATOR'S REF.		SECURITY CLASS.
	TP 96312 U		**Unclassified**

ORIGINATOR
National Aerospace Laboratory NLR, Amsterdam, The Netherlands

TITLE
Propeller-wing interference effects at low speed conditions

PRESENTED AT
the DLR Braunschweig Workshop on "Aspects of Engine-Airframe Integration for Transport Aircraft".

AUTHORS	DATE	pp	ref
L.G.M. Custers	**961020**	**21**	**8**

DESCRIPTORS

Aerodynamic characteristics
Body-wing configurations
Engine airframe integration
Propeller slipstreams
Semispan models
Thrust measurement
Wind tunnel tests

ABSTRACT

This paper describes propeller-wing interference measurements on a half model installed in the 3 by 4 meters Indonesian Low Speed Wind Tunnel (ILST). The wing of the model had a 2.1 meter (semi) span on which a nacelle and a 70 cm diameter propeller were mounted. To study the interaction effects with higher lift coefficients a flap could be mounted, covering about 70% of the span. Wing, flap and fuselage were all extensively equipped with pressure taps. Forces and moments measurements were performed by both an external balance, measuring the overall model loads, and a rotating shaft balance (RSB), measuring the propeller forces and moments.

The simultaneous use of a RSB and an external balance provided the opportunity to determine the interaction forces on both propeller and airframe. This combination of thrust/drag measurements with the RSB and the external balance was used in a set of bookkeeping procedures to determine the installed thrust, drag and the changes in thrust and drag when compared with the isolated propeller and the blades-off configuration. By using the RSB it was also possible to determine the propeller contributions to the other overall force- and moment-components such as the lift force and pitching moment.

The magnitude of the interference effects is illustrated by test results on a flaps-in configuration for a thrust coefficient of T_c = 2.5.

Contents

(21 pages in total)

PROPELLER-WING INTERFERENCE EFFECTS AT LOW SPEED CONDITIONS

L.G.M. Custers

National Aerospace Laboratory NLR
P.O. Box 90502
1006 BM Amsterdam, The Netherlands

ABSTRACT

This paper describes propeller-wing interference measurements on a half model installed in the 3 by 4 meters Indonesian Low Speed Wind Tunnel (ILST). The wing of the model had a 2.1 meter (semi) span on which a nacelle and a 70 cm diameter propeller were mounted. To study the interaction effects with higher lift coefficients a flap could be mounted, covering about 70% of the span. Wing, flap and fuselage were all extensively equipped with pressure taps. Forces and moments measurements were performed by both an external balance, measuring the overall model loads, and a rotating shaft balance (RSB), measuring the propeller forces and moments.

The simultaneous use of a RSB and an external balance provided the opportunity to determine the interaction forces on both propeller and airframe. This combination of thrust/drag measurements with the RSB and the external balance was used in a set of bookkeeping procedures to determine the installed thrust, drag and the changes in thrust and drag when compared with the isolated propeller and the blades-off configuration. By using the RSB it was also possible to determine the propeller contributions to the other overall force- and moment-components such as the lift force and pitching moment.

The magnitude of the interference effects is illustrated by test results on a flaps-in configuration for a thrust coefficient of $T_c = 2.5$.

NOMENCLATURE

b/2	semi span of the half model	(m)
c	chord	(m)
$\bar{c}$	mean aerodyamic chord	(m)
c_l	local lift coefficient = l /q c	
C_D	drag coefficient = D /q S_w	
C_L	lift coefficient = L /q S_w	
C_M	pitching moment coefficient = moment/q S_w b/2	
D	drag, diameter	(N)
D_{bp}	backplate force	(N)
F_{exb}	external balance force in model axial direction	(N)
F_{rsb}	rotating balance axial force	(N)
F_N	normal force	(N)
J	advance ratio = V_∞/N D_p	
L	lift force	(N)

l	local lift	(N/m)
N	rotational speed	(rps)
q	dynamic pressure	(N/m^2)
S	area	(m^2)
T	propeller thrust	(N)
T_c	thrust coefficient = propeller axial thrust/q S_p	
V_∞	tunnel velocity	(m/s)

η	propeller efficiency
$\Delta\eta$	difference in installed and isolated efficiency = η_{inst}-η_{iso}

subscripts

ax	axial
b	body
fa	free air
inst	installed
iso	isolated
j	jet
n	nacelle
p	propeller, propulsive
s	slipstream
sh	shaft
w	wing
wn	wing+nacelle (in the blades-on configuration)
wnp	wing+nacelle+propeller
wn0	wing+nacelle (in the blades-off configuration)

INTRODUCTION

Interference effects on a wing or a wing/flap combination and the propeller installation are especially important at low speed conditions like climb with one-engine inoperative and go-around. The effect of wing sweep and increased wing-upwash due to large lift coefficients will affect the propulsion installation. A propeller will in such conditions generate off-axis forces and contribute to the pitching moment as well as the yawing moment. The slipstream will affect the wing or wing/flap combination. Nacelle pressure drag and friction drag will increase, and the slipstream swirl recovery will induce a thrust component on the wing.

In a joint Indonesian/Dutch[1] effort an experimental investigation was performed to provide more insight into the magnitude of the above mentioned effects on a typical transonic configuration for a low speed condition (wing sweep, high lift, flap extension).

For this investigation a half-model test set-up was designed and manufactured for installation

[1] The partners are in the Joint Research Program JR-01 are : Pt. Industri Pesawat Terbang Nusantara, (IPTN); Laboratory for Aero-, Gas-dynamics and Vibrations (LAGG) of Indonesia; Fokker Aircraft B.V.; Technical University of Delft (TUD); and the National Aerospace Laboratory (NLR) of the Netherlands

in the 3 by 4 meters Indonesian Low Speed Wind Tunnel (ILST) of LAGG in Serpong, Indonesia. This paper briefly describes the test set-up and will discuss the interference effects as found by the experimental investigation.

TEST SET-UP

Test facility

The test was performed in the ILST, an atmospheric closed-circuit wind tunnel. It has a closed test section with a rectangular cross section of 4 m wide and 3 m high and a length of 8.75 m. The ILST has a design operating range of 0 to 110 m/s. The test section is equipped with a six-component external balance. A lay-out of the ILST is provided in figure 1.

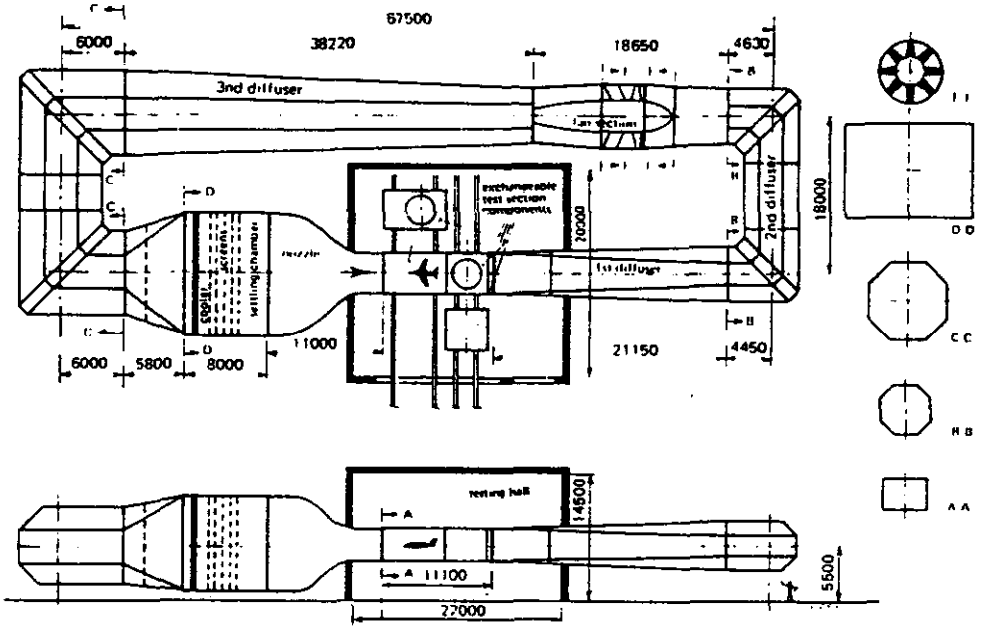

Figure 1 Lay-out of the ILST.

Model description

The half model consisted of 5 main components; wing, flap, nacelle, propeller and fuselage body, a tailplane was not included. The wing and body formed the basic configuration, onto which the other components could be mounted in any combination. In figure 2 the tested configurations are drawn and figure 3 shows the model in the test section. The model has been designed by Fokker Aircraft B.V. and was manufactured by LAGG and IPTN, with structural design support by NLR. The wing has a half-span of 2.1 m and is equipped with nine pressure stations each with 50 pressure orifices. In addition the wing houses the air feed and the instrumentation cabling for the air motor as well as pressure tubing for the pressure stations. A plastic zigzag tripping strip was glued onto the upper and lower wing

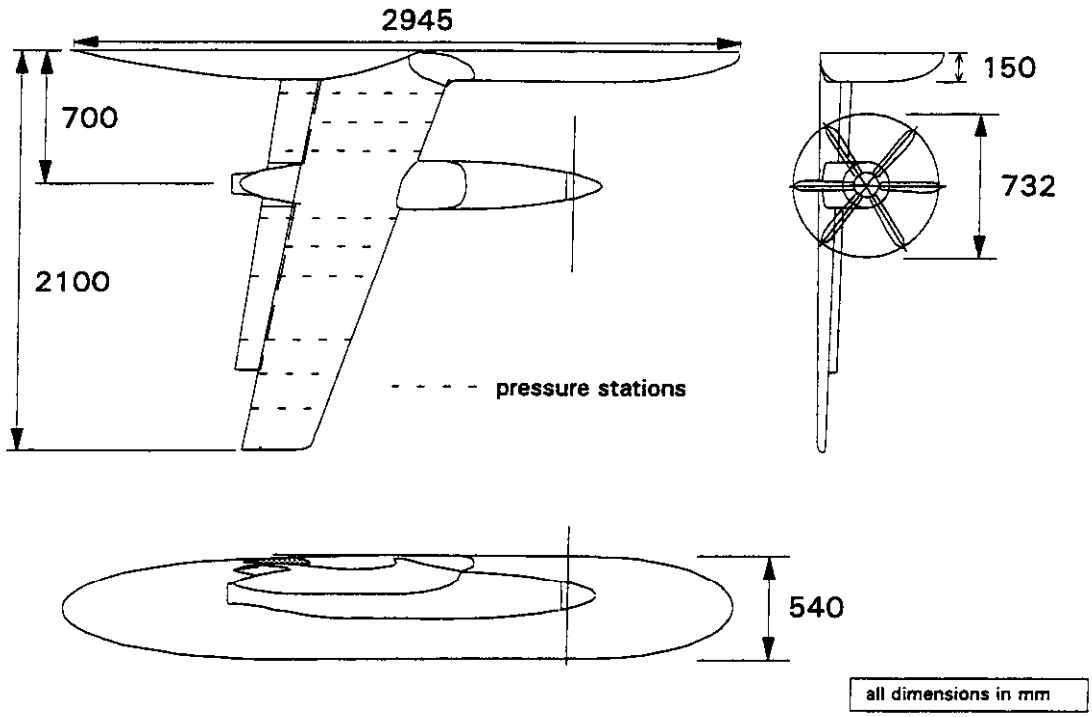

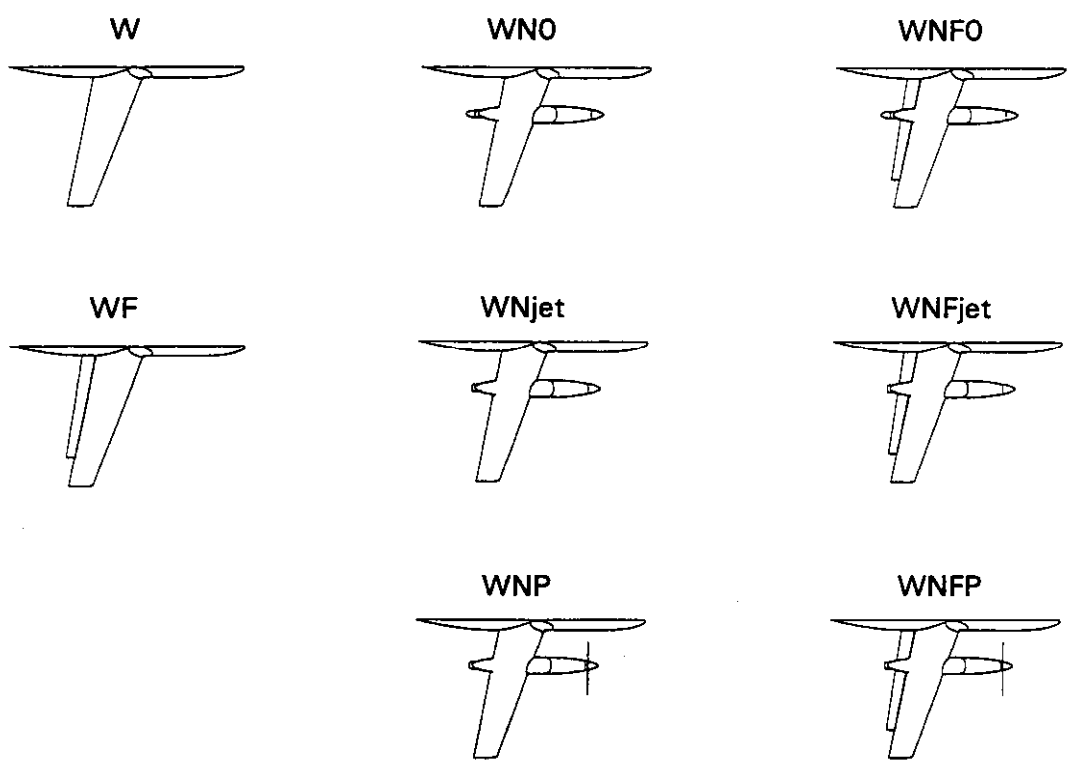

Figure 2 Basic configurations of the model.

Figure 3a Front view of the model installed in the test section.

Figure 3b View on the downside of the model.

surface across the entire span in order to fix the transition at 10% local chord on the upper surface and 30% on the lower surface.

A single slotted flap from 7% to 80% wing span can be installed with a flap angle of 15 degr.. To enable installation of the nacelle the flap is divided into two parts, a small third part is used to close the gap when the nacelle is not installed. The flap is equipped with 5 pressure sections each with 30 pressure orifices (see figure 2).

The nacelle houses the drive unit and exhaust. The drive unit can be subdivided, depending on the configuration, into the TDI 1555 air turbine motor, slipring unit, two flexible couplings and supportive bearings. The TDI 1555 is capable of delivering 150 kW at 7500 rpm. The slipring is equipped with 28 channels and is manufactured by IDM. To drive the air motor, pressurized air was supplied to the model through the ILST high pressure air system. The exhaust is shaped as a standard ASME nozzle and total temperature and total pressure rakes were placed just ahead of the exhaust plane. The air turbine motor can be replaced by a throttle plate which is used for simulation of natural blowing and for exhaust calibrations. To determine the jet interference effects a faired plug could be placed in the exhaust during blades-off drag measurements, see also figure 2.

The model propeller is a 1:5 scaled version of the 6-bladed Fokker 50 propeller and has a diameter of 0.732 m. The propeller rotates inboard-up, clockwise when viewed from behind. The propeller blades were mounted in an aluminium hub connected to the outer ring of the rotating shaft balance. To be able to account for the pressure term acting on the aftside of the hub (thus also measured by the RSB), a "backplate" was added to the rotating hub, and a plate equipped with pressure taps was mounted to the front end of the nacelle.

A four-component rotating shaft balance (RSB) was mounted between the drive shaft and propeller hub. This RSB has been developed and manufactured at NLR for maximum loads of 1250 N, 125 Nm, 600 N and 40 Nm for resp. the axial force, torque and the off-axis force and moment. By using a 24-channel 16-bit FFT-system the off-axis components can be decomposed into normal-/sideforce and yaw-/pitching moment. A magnetic sensor incorporated in the air turbine motor was used as an azimuth marker for the decomposition of the forces and moments. A more extensive discussion on the design and usage of the RSB is given in [1,2].

The fuselage body was shaped to simulate in a simple way a high-wing configuration. The body itself was installed at 5 cm distance from the tunnel wall, a non-metric peniche was used to fill this gap. To minimise flow leakage from the downside to the topside of the body, a labyrinth seal was installed in the peniche. The fuselage was equipped with three pressure stations in streamwise direction on the external surface. The model, was mounted on the six-component external balance and can be rotated about y-axis of the external balance for angle-of-attack variations.

TEST PROGRAM

Four main configurations were measured; wing alone (W), wing+flap (WF), wing+nacelle (WN), and wing+nacelle+flap (WNF). For the WN and WNF configurations blades-on and

blades-off configurations have been measured (resp. WNP and WNFP). In the blades-off configurations both blowing nozzle (WNjet, WNFjet) and faired nozzle (WN0, WNF0) were measured. For most configurations the propeller was set at a blade pitch angle of 28 degr. at 70% blade radius. Flap angle setting for the WF and WNF configurations was 15 degr.. The measurements were performed by making angle-of-attack sweeps at constant tunnel velocity (40, 70 and 80 m/s), and constant thrust coefficient or nozzle pressure ratio (in case of the blowing nozzle configuration). A constant thrust coefficient could be obtained by adjusting the propeller rpm using the RSB on-line propeller shaft thrust data.

In this paper the demonstration of the interference effects is limited to the comparison between the basic flaps-in configuration WN0 and the flaps-in,blades-on configuration WNP. The comparison was made for a thrust coefficient of 2.5 .

BOOKKEEPING

Due to the large number of tested configurations and the combined use of a RSB and external balance, it is possible to study the aerodynamic characteristics of the individual components, their mutual interference, and the overall aerodynamics characteristics. Since the bookkeeping is applied to a half model, only the symmetric components: lift, drag and pitching moment, are discussed. In the following *lift* relates to all aerodynamic forces in the lift direction (perpendicular to the tunnel flow), including the contribution from the propeller. The *drag* relates to all aerodynamic forces in streamwise (drag) direction, excluding the streamwise components of the propeller and jet thrust forces.

Lift

The various configurations each generate lift which is a summation of both the lift generated by the basic model components and the lift in- or decrements generated by the mutual interferences between the components. When placed in the oblique flow in front of the wing the propeller will also contribute to the lift force. This contribution is a vector summation of the propeller axial thrust and the propeller normal force:

$$L_p = T_{ax}\sin\alpha + F_{N_p}\cos\alpha$$

With a bookkeeping scheme which uses the results of both the external and rotating balance measurements, as well as the results of the measurements on the different configurations, it is possible to distinguish the different lift components from the airframe and the propeller.

Table 1 provides an overview of the applied bookkeeping scheme. It shows for example that subtracting the propeller lift L_p (as measured by the RSB) from the overall lift L_{wnp} of the WNP configuration (measured by the external balance), provides the lift of the wing and nacelle L_{wn}. Similarly the other basic components and interferences are determined. Note that the matrix has some implicit bookkeeping which is not shown in order to maintain a good overview. For instance ΔL_n is the increase in lift force when mounting the nacelle plus faired plug on the wing (the WN0 configuration). When mounting the propeller (configuration WNP) changes in the nacelle lift increment ΔL_n, due to subsequent interference effects of respectively the exhaust jet and the propeller slipstream, are incorporated into respectively

the exhaust jet lift increment ΔL_j and the slipstream lift increment ΔL_s. Such "mutual" interferences cannot be determined with this set-up.

	measured by the external balance				measured by the RSB	
configuration :	W	WN0	WNjet	WNP	P_{inst}	P_{iso}
generates : subtract :	L_w	$L_{wn0} = L_w + \Delta L_n$	$L_{wnj} = L_w + \Delta L_n + \Delta L_j$	$L_{wnp} = L_w + \Delta L_n + \Delta L_j + L_p + \Delta L_s$	$L_p = L_{p0} + \Delta L_p$	L_{p0}
W		ΔL_n	$\Delta L_n + \Delta L_j$	$\Delta L_n + \Delta L_j + L_p + \Delta L_s$		
WN0			ΔL_j	$\Delta L_j + L_p + \Delta L_s$		
WNjet				$L_p + \Delta L_s$		
WNP						
P_{inst}				$L_{wn} = L_w + \Delta L_n + \Delta L_j + \Delta L_s$		
P_{iso}					ΔL_p	
WN0 + P_{inst}				$\Delta L_s + \Delta L_j$		
WNjet + P_{inst}				ΔL_s		

Table 1 Lift bookkeeping scheme

Thrust and drag

Similarly to the lift force, a bookkeeping approach must be applied to the forces in drag direction: thrust/drag bookkeeping. Various definitions are used in the literature to identify the thrust of the propeller; free air thrust, propulsive thrust, shaft thrust, etc. The definition of the shaft thrust and propulsive thrust relates to the approach that in case of an installed propeller the airframe drag is counteracted by the streamwise thrust force acting on the shaft of the engine plus the streamwise (net) jet thrust. In this definition all drag increments on the airframe are captured as drag, whereas the thrust and thrust increments of the propeller are captured in the thrust acting on the shaft. The propulsive thrust is the net result of the shaft thrust and the slipstream induced drag increments (with respect to the drag of the blades-off configuration when compared at equal lift), and is measured by the external balance:

$$T_p = T_{sh} - \Delta D_s = F_{exb} - D_{wn0} + T_j$$

In which the blades-off drag (D_{wn0}) is determined from the external balance measurements on the WN0 or WNF0 configuration.

For the purpose of the thrust/drag bookkeeping the shaft thrust is defined as the streamwise component of the propeller shaft force :

$$T_{sh} = T_{ax}\cos\alpha - F_{Np}\sin\alpha$$

The propeller axial thrust T_{ax} is determined by correcting the RSB measurements for the internal backplate force :

$$T_{ax} = -(F_{rsb} - D_{bp})$$

Thus when combining external balance and RSB measurements, the shaft thrust and the propulsive thrust can be determined directly and result into a matrix for the thrust/drag bookkeeping, shown in table 2.

In the determination of the different drag and thrust components the thrust of the exhaust jet is subtracted for both cases with an exhaust jet present (WNjet and WNP), and is therefore not shown in the result of the bookkeeping. By using a velocity coefficient c_v database determined during seperate nozzle calibrations performed by NLR, the exhaust thrust T_j was calculated by :

$$T_j = c_v V_j \dot{m}$$

In which the ideal jet velocity v_j was determined from the temperature and pressure measurements at the exhaust measurement station, and the mass flow $\dot{m}$ by a sonic venturi installed in the high pressure air supply system.

	measured by the external balance				measured by the RSB	
configuration :	W	WN0	WNjet	WNP	P_{inst}	P_{iso}
generates :	D_w	$D_{wn0} = D_w + \Delta D_n$	$T_j - D_{wnj} = T_j - D_w + \Delta D_n + \Delta D_j$	$T_{sh} + T_j - D_{wnp} = T_{sh} + T_j - (D_w + \Delta D_n + \Delta D_j + D_p + \Delta D_s)$	$T_{sh} = T_{sh0} + \Delta T_{sh}$	$T_{sh0} = T_{fa} + \Delta T_b$
subtract :						
WN0			ΔD_j	$T_p = T_{sh} - (\Delta D_j + \Delta D_p + \Delta D_s)$		
WNjet				$T_p = T_{sh} - (\Delta D_p + \Delta D_s)$		
P_{inst}				$D_{wn} = D_w + \Delta D_n + \Delta D_j + \Delta D_s$		
P_{iso}					ΔT_{sh}	
WN0 + P_{inst}				$\Delta D_s + \Delta D_j$		
WNjet + P_{inst}				ΔD_s		

Table 2 Thrust and drag bookkeeping scheme

As shown in table 2 the slipstream induced drag term can be determined by comparing the

shaft thrust and propulsive thrust, using the data from both the RSB and the external balance:

$$\Delta D_s = T_{sh} - T_p$$

Pitching moment

The bookkeeping scheme for the pitching moment is identical to that of the lift and is not shown here.

DEMONSTRATION OF INTERFERENCE EFFECTS

Using the bookkeeping scheme presented in tables 1 and 2, the interference effects can be demonstrated by a comparison between the WN0 and WNP (at T_c = 2.5) configurations. In doing so the interference effects of the nozzle jet (ΔL_j and ΔD_j) are neglected. They are small, however, and for the purpose of the discussion this approach is acceptable.

First interference effects on the airframe in terms of lift, drag and pitching moment will be discussed followed by an analysis of the lift contribution of the propeller and the propeller efficiency.

Airframe

Lift

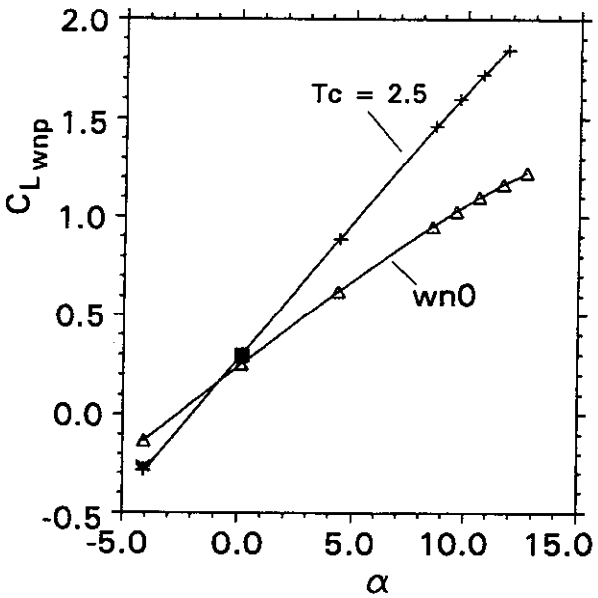

Figure 4 Comparison of blades-on and blades-off lift curves.

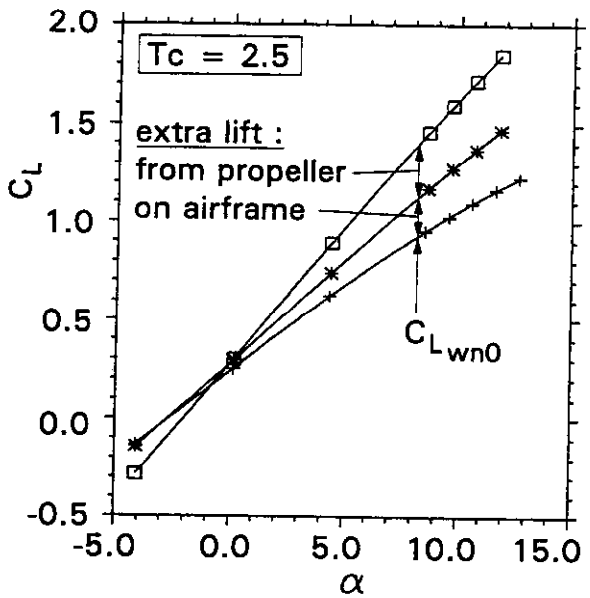

Figure 5 Breakdown of the lift at a constant thrust coefficient of 2.5 .

For the blades-off configuration the lift coefficient at 12 degr. angle-of-attack is about 1.2. By installing the propeller the overall lift coefficient (i.e. the lift generated by the wing/nacelle/propeller combination) increases to about 1.9 at the same angle-of-attack, as can be observed in figure 4, an increase in overall lift ΔC_{Lwnp} of 0.7 . Figure 4 also shows that the lift interference changes of sign at negative angles-of-attack.

Due to the mutual interference and the effect of angle-of-attack on the propeller forces, both the wing+nacelle and the propeller will contribute to the lift increase. As can be seen in figure 5 the larger part of the lift increase is generated by the propeller. At a thrust coefficient of 2.5 and an overall lift coefficient C_{Lwnp} of 1.0 the propeller generates about 18% of the lift. Clearly the influence of the propeller is significant and one should be careful to fully appreciate this propeller contribution, instead of (partly) attributing it to the lift increase generated by the wing+nacelle.

The stall delaying effect of the slipstream on the lift of the wing+nacelle C_{Lwn} is visible in figure 5 the curve remains linear to higher angles-of-attack for a thrust coefficient of 2.5 . For the blades-off configuration the flow seperation begins at the inboard part of the wing, as shown by oil visualisation. This part is subject to a larger velocity, both inside and outside the slipstream. The combination of large velocities in the slipstream and the presence of a "gulley" between the nacelle and fuselage creates a local increase in velocity, resulting in higher local lift. The airframe parts immersed in the slipstream are subject to increased velocities and to the local variations in angle-of-attack, due to the swirl in the propeller slipstream. Directly outboard of the nacelle the local inflow angles are reduced, resulting in lower lift coefficients. The large lift increase on the inboard parts of the wing more than offsets this lift loss. The outside part of the wing is hardly affected by the presence of the propeller (see figure 6).

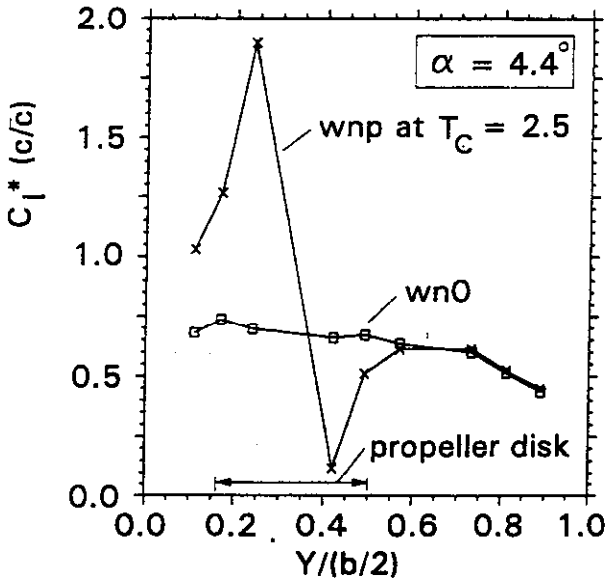

Figure 6 Influence of the slipstream on the spanwise lift distribution.

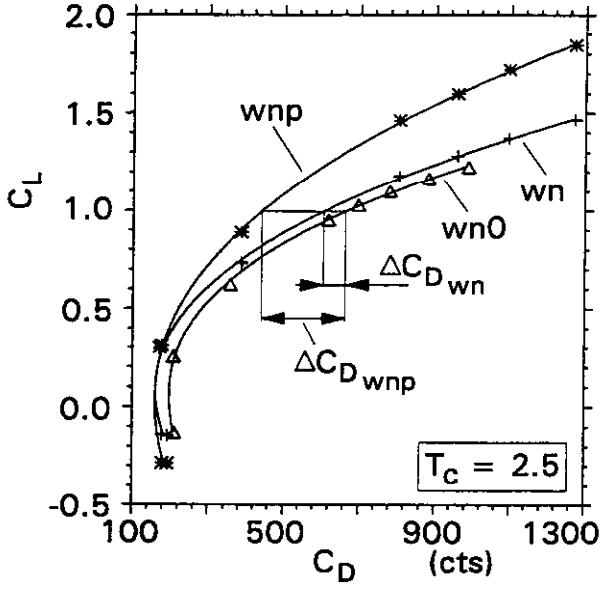

Figure 7 Comparison and breakdown of the lift-drag curve.

Drag

As was discussed previously the use of the RSB in combination with an external balance permits a direct analysis of the drag of the wing+nacelle combination. For the purpose of analysis it is useful to make a comparison of the following lift versus drag curves:
- the blades-off lift-drag curve (using C_{Lwn0} vs. C_{Dwn0}),
- the blades-on overall lift-drag curve (using C_{Lwnp} vs C_{Dwnp}),
- the blades-on wing+nacelle lift-drag curve (using C_{Lwn} vs C_{Dwnp}).

From the comparison in figure 7 it is observed that the favourable inboard-up rotation of the propeller and the lift contribution of the propeller effectively lower the drag when compared on basis of the same lift coefficient. For lower lift coefficients the reduction is smaller.

As shown in figure 7 the comparison of the drag at the same lift coefficient yields the following drag increments :
- ΔC_{Dwnp} from the comparison of the C_{Lwnp}-C_{Dwnp} and the C_{Lwn0}-C_{Dwn0} curves,
- ΔC_{Dwn} from the comparison the C_{Lwn}-C_{Dwnp} and the C_{Lwn0}-C_{Dwn0} curves.

By studying these drag increments the interference effects become more clearly observable. The variation of the drag increments ΔC_{Dwnp} and ΔC_{Dwn} with respectively C_{Lwnp} and C_{Lwn} are shown in figures 8 and 9. Both show a reduction in drag due to the slipstream interference. Figure 8 shows that the variation with increasing lift coefficient is very small up to lift coefficient of 0.5, after which the drag decreases by 375 counts (see figure 8).

As shown in figure 9 ΔC_{Dwn} is nearly constant up until a lift coefficient of about 0.7 after which the drag reduction becomes almost 100 counts. Apparently the increase of friction drag and pressure drag on the immersed parts of the wing are offset by the swirl recovery

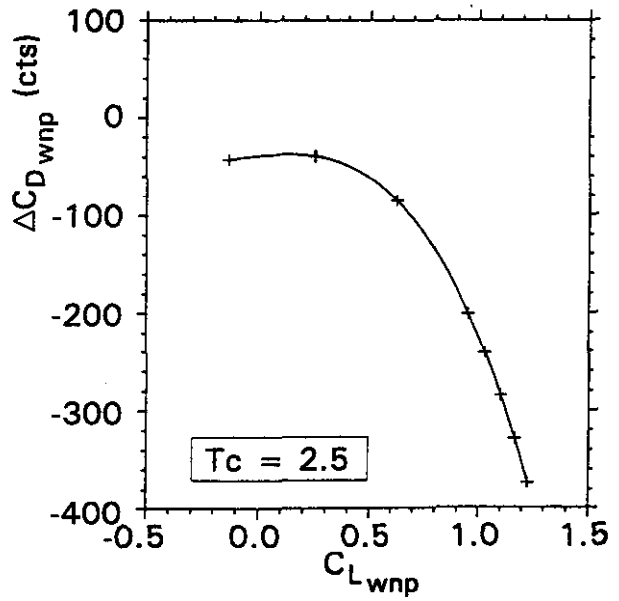

Figure 8 Change of drag due to slipstream interference with respect to the overall lift.

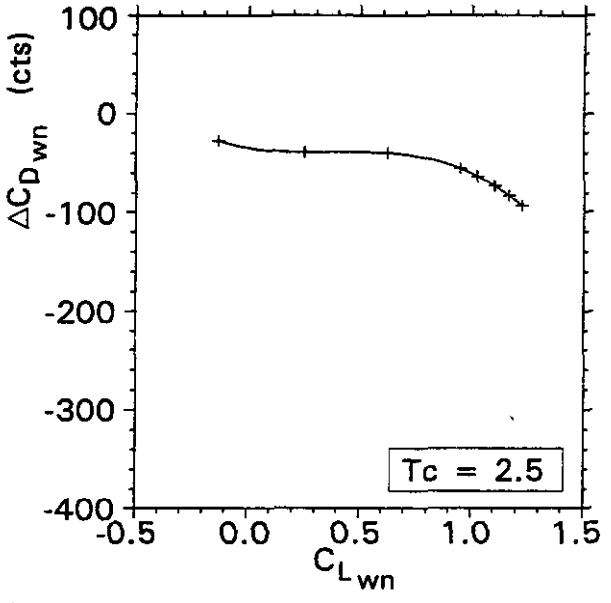

Figure 9 Drag changes due to slipstream with respect to the lift acting on the wing+ nacelle.

due to the larger forward rotation of the lift vector at the inboard part of the wing than the rearward rotation at the outboard parts [7].

The large drag reductions shown in figure 8 are mainly attributed to the influence of a lower angle-of-attack in the blades-on condition. To retain the same overall lift a lower angle-of-attack is needed than for the blades-off configuration because the propeller contributes a significant part to the overall lift. For the tested configuration this effect is larger than the reduction of the drag of the wing+nacelle due to the slipstream effects, as observed from the comparison of the blades-on and blades-off conditions (see figures 8 and 9).

Pitching moment

The pitching moment (without tailplane) becomes positive when adding the propeller (see figure 10). Both the propeller lift and thrust contribute to a positive (nose-up) pitching moment due to the relative position of the propeller to the model reference point (see figure 2). This is confirmed by the breakdown of the pitching moment as given in figure 11. Note the indifferent behaviour of the pitching moment generated by the wing and nacelle (C_{Mwn}). The pitching moment of the propeller is small.

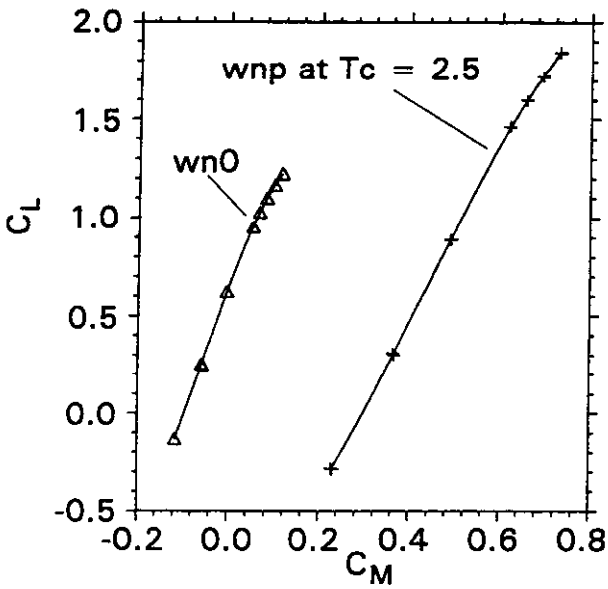

Figure 10 Change of the overall pitching moment.

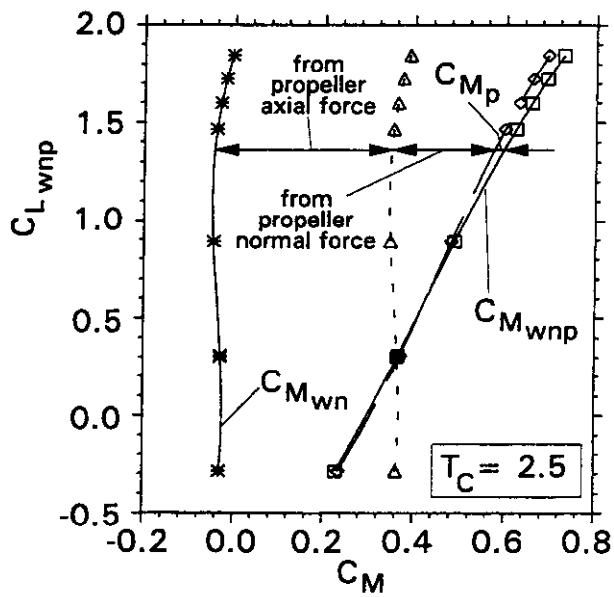

Figure 11 Breakdown of the pitching moment for a constant thrust coefficient of 2.5 .

Propeller

Lift

It is useful to study the lift contribution of the propeller, and to identify the relative importance of the normal and axial force components of the propeller shaft force. In figure 12 these two contributions are drawn; the contribution of the axial thrust component is somewhat larger than the normal force component. When installed in front of the wing the propeller will experience different inflow angles compared to the isolated case. This will

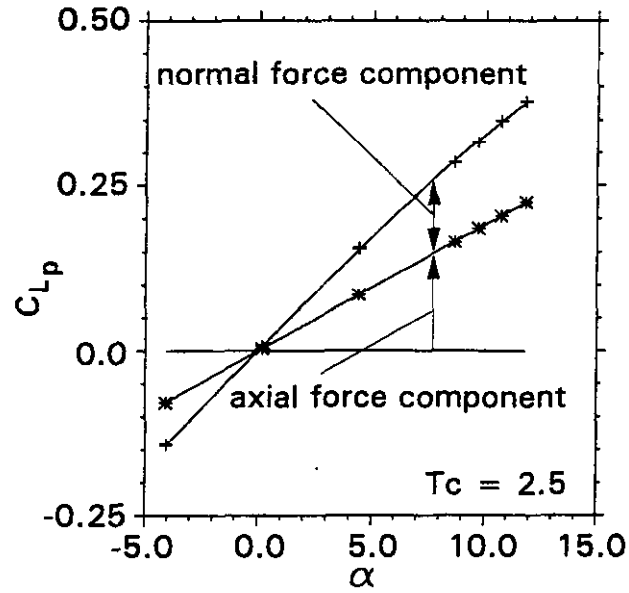

Figure 12 Contributions of the axial thrust component and the normal force component to the propeller lift.

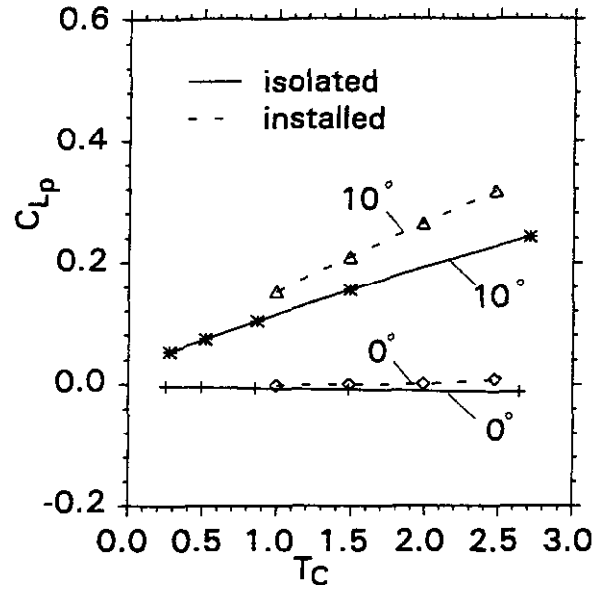

Figure 13 Propeller lift of the installed and isolated propeller.

change the propeller lift, generated at a particular thrust coefficient and it will change the streamwise efficiency. In figure 13 and 14 the changes in lift and efficiency for the isolated and installed case are compared at different angles-of-attack. The increased upwash in front of the wing results in larger propeller lift (see α= 10 degr.). The propeller efficiency, based on the thrust in streamwise direction, is lower compared to the isolated propeller. An analysis of the overall aircraft performance, using the changes in drag and propeller efficiency , should be made to determine the final performance gain or loss, but is outside the scope of this paper.

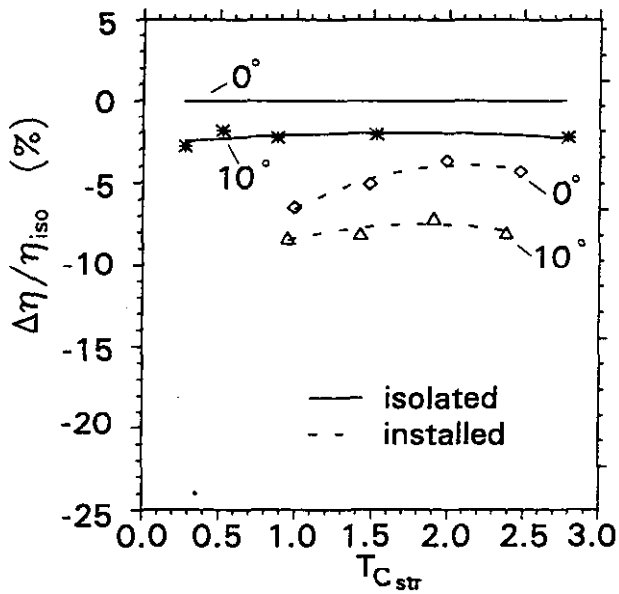

Figure 14 Difference of installed and isolated efficiency of the propeller.

CONCLUDING REMARKS

In the Indonesian/Dutch cooperation programme a valuable wind tunnel model for the investigation of propeller-wing interference effects has been manufactured and tested. A limited discussion of some test results has been made to show the benefits of a combined use of a rotating shaft balance and an external balance. It enables the determination of the interference effects between the propeller and the airframe.

For the analysed configuration with $T_c=2.5$ and at an overall lift coefficient of $C_{Lwnp}=1.0$, about 18% of the overall lift was contributed by the propeller. The contribution of the lift component of the axial thrust to the lift of the propeller is slightly larger than the contribution of the propeller normal force. Since the lift of the propeller is measured directly, the lift generated by the airframe (wing +nacelle) can be determined easily, without any theoretical corrections.

Because the streamwise thrust component of the propeller is determined by the rotating shaft balance, the drag of the airframe can be calculated directly from the external and rotating shaft balance measurements. Compared at a constant thrust coefficient of 2.5 the drag of the airframe decreases for increasing lift. The swirl recovery and the increasing lift contribution of the propeller, requiring less lift from the airframe itself with lower induced drag, both result in lower overall drag levels.

A breakdown of the pitching moment has been performed, accounting for the contribution of the propeller, which provides the pitching moment of the airframe. For the flapless configuration the airframe itself is indifferent in pitching moment for varying thrust levels.

In the near future the results of the measurements will be analysed in more detail by the partners is this joint effort. The results will help to obtain improved knowledge on interference effects and will provide a valuable database for the validation of computational codes. Further out in the future follow-on measurements will most probably be performed, aimed at providing additional information such as interference effects with larger flap deflections and flow field data behind the propeller disk.

ACKNOWLEDGEMENTS

The data discussed here are the result of a joint effort of the entire team of JR-01; the people at ITPN, Fokker, LAGG, TU Delft and NLR. Especially the people of LAGG have performed a great effort during the measurements. Also acknowledgements must be made to S. J. van der Pijl, who has analysed the data during his internship at NLR, and to W.B. de Wolf and J. van Hengst, who provided valuable comments during the preparation of this paper.

REFERENCES

[1] L.G.M. Custers, Experience with rotating shaft balances for measurements of total propeller force and moment, Indonesian Aircraft Propulsion Symposium 1994, February 1994.

[2] L.G.M. Custers, A.H.W. Hoeijmakers, A.E. Harris, Rotating shaft balance for measurements of total propeller force and moment, 15th International Congress on Instrumentation Aerospace Simulation Facilities, June 1993

[3] G. Fratello, D. Favier, C. Maresca, Experimental and numerical study of the propeller/fixed wing interaction, Journal of Aircraft, June 1991.

[4] H. Muhammad, Identification of turboprop thrust from flight test data, PhD-Thesis, Technical University of Delft, December 1995.

[5] J.D. Price, M.H. Aston, I.F. Burns, Propfan integration on an advanced wing, International forum on Turbine Powered Simulation at DNW, May 1995

[6] G.J. Schipholt, et all, Investigation of methods for modelling propeller-induced flow fields, AIAA 93-0874, January 1993.

[8] L.L.M. Veldhuis, D.W.E. Rentema, Quantative wake surveys behind a tractor propeller-wing configuration, AIAA 95-3908, September 1995.